RSC Advances

PAPER

View Article Online
View Journal | View Issue

Cite this: *RSC Adv.*, 2022, **12**, 33276

Mesoporous acidic polymeric ionic liquids as novel solid acids for catalytic hydrolysis of ketoxime reactions†

Shanshan Zhao,[a] Zhengxiang Ma,[a] Peng Cheng,[a] Yanji Wang,[ab] Xinqiang Zhao,[ab] Qiusheng Yang,[ab] Junqi Zhang[a] and Dongsheng Zhang *[ab]

In this study, a series of mesoporous acidic polymeric ionic liquids were successfully synthesized and characterized to explore their structures and properties. Examination of catalytic performance using cyclohexanone oxime's maximum conversion were investigated, and the Box–Behnken design was used to achieve the highest hydrolysis conversion. Excellent catalytic activity, structural stability, and an easy recovery feature were all displayed by the Poly(VBS-DVB)HSO_4 catalyst. Additionally, a possible reaction pathway involving hydrogen protons was proposed for the present hydrolysis. Moreover, a series of ketoximes were also examined including acetone oxime, butanone oxime, cyclopentanone oxime and acetophenone oxime over Poly(VBS-DVB)HSO_4 catalyst. The conversion of ketoxime was not less than 80.44%, and the results also demonstrated excellent catalytic performance. Synthesis of mesoporous acidic polymeric ionic catalysts with good properties would be very important for their applications.

Received 12th October 2022
Accepted 15th November 2022

DOI: 10.1039/d2ra06422g

rsc.li/rsc-advances

1. Introduction

Hydroxylamine and its salts are important chemical intermediates, which are mainly in the form of hydroxylamine sulfate, hydroxylamine hydrochloride, hydroxylamine nitrate and hydroxylamine phosphate.[1] These kinds of hydroxylamine are widely used in the production of ε-caprolactam, medicine, pesticides, rubber, dyes, military, and so on.[2–4] Traditional ways for the production of hydroxylamine salt mainly include the Rashing method,[5] the hydroxylamine–phosphate–oxime (HPO) process,[6] the catalytic hydrogenation of nitric oxide[7] and acid hydrolysis of nitroalkanes, *etc.*[8] However, all these methods suffer from some problems including complicated operation processes, harsh reaction conditions and environmental pollution. Therefore, it is necessary to explore a mild and environment-friendly production route for hydroxylamine.

Additionally, hydroxylamine can also be produced by hydrolysis reaction using ketoxime as raw material, especially cyclohexanone oxime hydrolysis.[9] However, the industrial production of cyclohexanone oxime has been carried out with hydroxylamine salts as raw material for a long time. Therefore, the hydrolysis of cyclohexanone oxime to make hydroxylamine was once considered uneconomical. With the introduction of titanium silicon molecular sieve (TS-1) catalyst, the one-step synthesis of cyclohexanone oxime from cyclohexanone, NH_3, and H_2O_2 had recently become more developed and industrialized.[10] So that cyclohexanone oxime can be produced without using hydroxylamine,[9,11] thereby breaking the situation of traditional hydroxylamine synthesis of cyclohexanone oxime.[12] Therefore, it is reasonable and feasible to explore the hydrolysis of cyclohexanone oxime to hydroxylamine.

Usually, cyclohexanone oxime conversion is nearly 100% with inorganic acid as a catalyst.[8] Although the catalytic effect is satisfactory, there is still the problem of difficult catalyst recovery. Therefore, it is of great significance to develop a nonhomogeneous catalyst with high catalytic activity for the hydrolysis reaction. Ionic liquids (ILs), being a new type of solvent and catalyst with the advantages of designability, low volatility, good thermal stability as well as adjustable controlled acidity and alkalinity,[13,14] are widely used in organic synthesis, catalysis, gas separation and other fields.[15,16] Unfortunately, it has several drawbacks in terms of separation and recycling.[17,18] In recent years, the reactivation and reuse of ILs have attracted extensive attention.[19] Immobilization of ionic liquids has become a trend.[20] Many researchers have used chemical methods to immobilize ionic liquids on various catalyst carriers, such as silica gel,[21] activated carbon,[22] molecular sieve,[23] *etc.* ILs loaded on porous materials is an effective catalyst with good reusability. However, ionic liquids are generally only present on the surface of the carrier as they are covalently linked to the carrier's active group. This results in a low loading of ionic liquids and fewer active sites.[24,25] In our previous

[a]*Hebei Provincial Key Lab of Green Chemical Technology and High Efficient Energy Saving, Hebei University of Technology, Tianjin 300130, China. E-mail: zds1301@hebut.edu.cn; Fax: +86-22-60204294; Tel: +86-22-60204294*

[b]*Hebei Industrial Technology Research Institute of Green Chemical Industry, Huanghua 061100, Hebei, China*

† Electronic supplementary information (ESI) available. See DOI: https://doi.org/10.1039/d2ra06422g

studies, we also found a similar situation, which led to the low conversion of cyclohexanone oxime hydrolysis to hydroxylamine.[26] Therefore, we need to continue to find a solid acid to change the status of this reaction.

Recently, polymeric ionic liquids (PILs), a new type of polymeric material, are beginning to appear in public view. It combines the advantages of ILs and polymers, usually in solid form, with ionic liquid units in each polymer backbone. Functional PILs containing different functional groups and active sites are obtained through the modulated design of ILs monomers and ion exchange.[27,28] PILs with different functionalities shows good application prospects in polyelectrolyte,[29–31] adsorption and separation,[32,33] catalyst,[34–36] *etc.* PILs have received additional attention, particularly in the area of catalysis. Qiu *et al.* prepared polymeric self-curing ionic liquids as efficient catalysts for biodiesel production by a one-step process.[37] Dyson *et al.* described a polymeric ionic liquid (PIL) derived from trimethyl(*p*-vinyl benzyl)ammonium chloride ([VBTAm] Cl) efficiently catalyzes the *N*-carbonylation and *N*-methylation reactions of amines.[38] Sahiner *et al.* designed a polymeric ionic liquid catalyst of poly(4-vinyl pyridine) to replace the metal catalyst, which was successfully used for the hydrolysis of $NaBH_4$ and methanolysis to hydrogen.[39] Inspired by the above, in this work, we have introduced crosslinkers to synthesize a series of mesoporous acidic polymeric ionic liquids with exposed active sites and used in the hydrolysis of cyclohexanone oxime reaction. In addition, response surface methodology (RSM) was used to optimize the hydrolysis reaction parameters and the reusability performance of the PILs was examined.

2. Experimental

2.1. Materials

All reagents are analytical reagents and can be purchased directly without further purification. Divinylbenzene (DVB), *N*,*N*′-methylene bisacrylamide (MBA), 1-vinyl imidazole (vim), 1,3-propane sulfonate lactone, 1,4-butane sulfonate lactone, *n*-butyl bromide, azobisisobutyronitrile (AIBN), cyclohexanone oxime, cyclohexanone, butanone oxime, vutanone, acetone oxime, acetone, acetophenone oxime, acetophenone, chlorobenzene, trifluoromethanesulfonic acid and trifluoroacetic acid were purchased from Shanghai MACKLIN Company. Acetonitrile, ethyl acetate, ethanol, dichloromethane, dichloroethane, sulfuric acid, nitric acid, hydrochloric acid, phosphoric acid and potassium permanganate standard solutions were provided by Tianjin Chen Fu Reagent Factory.

2.2. Catalyst preparation

The method for the synthesis of acidic polymeric ionic liquids was based on the literature,[40] with modifications, and the specific synthesis steps were as follows.

2.2.1. Synthesis of ILs monomers. ILs monomers were synthesized by quaternization as follows. It was synthesized in a 100 mL three-necked flask. 1-Vinyl imidazole (0.05 mol, 4.7 g) was slowly mixed with 1,4-butane sulfonate (0.05 mol, 6.8 g) in an ice bath, and then stirred at 80 °C for 36 h. The formed solid was washed with acetonitrile and dried in a vacuum oven at 80 °C. The 1-vinyl-3-butane sulfonate imidazole (VBS) was obtained (Elemental analysis calcd: C 47.10 wt%, H 5.67 wt%, N 12.21 wt%, S 13.96 wt%. Found: C 44.64 wt%, H 5.53 wt%, N 11.24 wt%, S 11.21 wt%). Similarly, 1-vinyl imidazole-3-butylimidazole bromide salt (BuV) and 1-vinyl-3-propane sulfonate imidazole (VPS) were synthesized with the same procedure.

2.2.2. Synthesis of mesoporous acidic PILs precursors. The mesoporous acidic PILs precursors were prepared by free-radical copolymerization. Usually, VBS (2.5 g) was added into a solution containing 40 mL of ethanol and 5 mL of water with mechanically stirring for 5 min at room temperature. Then AIBN (0.075 g/3 wt%) and DVB (2.83 g) were added in turn and stirred mechanically at 80 °C for 6 h. After that, the mixture was filtered and washed sequentially with ethanol water three times. Finally, after being dried at 80 °C under vacuum for 10 h, the mesoporous PILs precursors were obtained and defined as Poly(VBS-DVB) (Elemental analysis found: C 64.10 wt%, H 6.39 wt%, N 5.46 wt%, S 4.57 wt%). The copolymer Poly(VPS-DVB) of VPS and DVB and the copolymer Poly(BuV-DVB) of BuV and DVB were obtained by the same procedure. MBA was used instead of cross-linking agent DVB, and the operation steps were the same as above. The copolymer poly of VBS and MBA (VBS-MBA), copolymer poly of VPS and MBA (VPS-MBA) and copolymer poly of BuV and MBA (BuV-MBA) were obtained respectively.

2.2.3. Synthesis of mesoporous acidic PILs. The above obtained mesoporous acidic PILs precursors Poly(VBS-DVB) was dispersed in 40 mL, 2.5 mol L^{-1} solutions of H_2SO_4 composed of ethanol–water, stirred for 12 h at room temperature, then filtered and washed repeatedly with CH_2Cl_2 until the pH value of filtrate was about 7. Subsequently, after being dried at 80 °C under vacuum for 6 h, the mesoporous acidic PILs were obtained and defined as Poly(VBS-DVB)HSO_4 (Elemental analysis found: C 31.69 wt%, H 5.11 wt%, N 1.25 wt%, S 10.01 wt%). Similarly, through the above procedures, Poly(VPS-DVB)HSO_4, Poly(BuV-DVB)HSO_4, Poly(VBS-MBA)HSO_4, Poly(VPS-MBA)HSO_4 and Poly(BuV-MBA)HSO_4 could be obtained respectively. The typical synthesis route of Poly(VBS-DVB)HSO_4 was shown in Scheme 1. Furthermore, sulfuric acid was replaced with different acids, and different acidic PILs including (Poly(VBS-

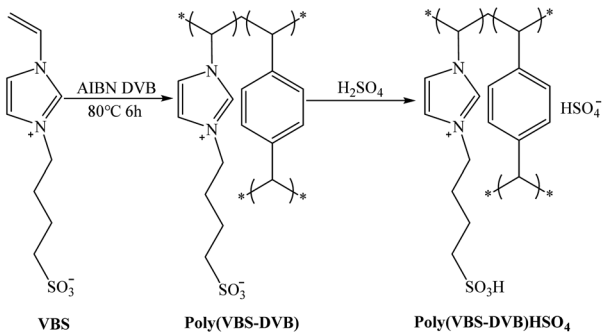

Scheme 1 Synthesis of acidic polymeric ionic liquids.

DVB)Cl, Poly(VBS-DVB)NO_3, Poly(VBS-DVB)H_2PO_4, Poly(VBS-DVB)$COOCF_3$ and Poly(VBS-DVB)SO_3CF_3) through the same steps. Table S1† summarized the synthesis of various ionic liquids functionalized on polymers.

2.3. Catalyst characterization

Fourier transform infrared (FT-IR) was recorded on a Nicolet NEXUS 470 (Thermoelectric Corporation, USA) to analyze the structure. The surface morphology of the samples was studied on a scanning electron microscope (Nova nano SEM 450, FEI, USA). Nitrogen adsorption–desorption isotherms were examined using a temperature-programmed chemisorption instrument (Auto Chem II 2920, Mac Instruments, USA). The surface area of the samples was measured by the Brunauer–Emmett–Teller (BET) method and the pore size distribution curves were calculated by the Barrett–Joyner–Halenda (BJH) method. The X-ray photoelectron spectroscopy (XPS) was studied with Mg Kα radiation on ESCALAB 250 spectrophotometer (Thermo Fisher Scientific Co., Ltd). Thermogravimetric analysis (TG) was performed under an N_2 atmosphere using the HCT-3 instrument (Beijing Hengjiu Scientific Instruments Factory). The CHNS elemental analysis was performed with a Flash EA Model 1112 (Thermoelectric Co, USA) instrument. Contact angle (CA) measurement using Data physics OCA 20 (Data physics, Germany) equipment. Nanoparticle size (DLS) was measured using a Zetasizer Nano ZS90 (Malvern manufacturer) device at 25 °C.

2.4. Catalytic testing

The cyclohexanone oxime hydrolysis reaction was carried out in a 100 mL eggplant-shaped bottle equipped with a reflux condenser. Usually, cyclohexanone oxime (0.5 g), catalyst (2 g) and water (55 mL) were added sequentially and stirred for 1 h at 60 °C. After that, the PILs catalyst was separated by centrifugation, and the separated PILs was washed with ethanol and dried under vacuum for further use.

The obtained organic phase was extracted with dichloroethane. The concentrations of organic components were analyzed by a 7890B gas chromatography. During the analysis process, chlorobenzene was selected as an internal standard. Fig. S1† shows a typical gas chromatogram. From this, it can be found that besides the organic product cyclohexanone, no other byproduct was observed. Cyclohexanone oxime conversion ($X_{\text{Cyo-o}}$) was calculated by the following. The hydroxylamine in the aqueous phase was analyzed by oxidation–reduction titration with potassium permanganate. The yield (Y_{NH_2OH}) and the selectivity of hydroxylamine (S_{NH_2OH}) were calculated as follows.

$$X_{\text{Cyo-o}} = \frac{n_{\text{Cyo}}}{n_{\text{Cyo-o}}} \times 100\% \quad (1)$$

$$Y_{NH_2OH} = \frac{(v_1 - v_2)\cdot 10^{-3}\cdot c\cdot \frac{5}{2}}{n_{\text{Cyo-o}}} \times 100\% \quad (2)$$

$$S_{NH_2OH} = \frac{Y_{NH_2OH}}{X_{\text{Cyo-o}}} \times 100\% \quad (3)$$

where: v_1 is the volume of potassium permanganate standard solution, v_2 is the volume of potassium permanganate standard solution in the blank test, c is the concentration of potassium permanganate standard solution, n_{Cyo} is the amount of cyclohexanone, and $n_{\text{Cyo-o}}$ is the amount of cyclohexanone oxime.

2.5. Experimental design

2.5.1. Experimental design methodology. In this experiment, the Box–Behnken design (BBD) method was adopted, and the conversion of cyclohexanone oxime was taken as the response target value. By observing the relationship between various variables and the reaction, the optimum conditions of cyclohexanone oxime hydrolysis were sought. Through the pairwise interaction between the three influencing factors, the influence of the three parameters on the hydrolysis efficiency of cyclohexanone oxime was analyzed, and the second-order functional relationship between the parameters and the target value was established, to obtain the theoretical optimal solution for the practical parameter optimization.

2.5.2. Experimental factors, levels and response. Experimental factors and levels were chosen according to literature data and experiences.[41,42] Table S2† shows these factors and levels. X_1 represents reaction temperature, X_2 represents catalyst amount, and X_3 represents water consumption. In the Box–Behnken design, the factors were set as three levels of the value range, *i.e.*, low level, medium level and high level, with "−1", "0" and "+1" as coding representatives, respectively. Cyclohexanone oxime conversion was used as the evaluation index for the test, and the response target value was expressed as Y. The experimental factors and coding levels were shown in Table S2.† The following model equations were used to analyze the response and variable interactions, as well as to predict the best values. The quadratic equation model was expressed according to eqn (4):

$$Y = \lambda_0 + \sum_{i=1}^{3} \lambda_i x_i + \sum_{i=1}^{3} \lambda_{ii} {x_i}^2 + \sum_{i<j}^{3} \lambda_{ij} x_i x_j \quad (4)$$

3. Results and discussion

3.1. Characterizations of catalyst

The chemical composition and chemical valence states of the synthesized Poly(VBS-DVB)HSO_4 were further evaluated by XPS. The XPS spectra (Fig. 1a) confirmed that the Poly(VBS-DVB)HSO_4 contains C, N, O and S elements, indicating that 1-vinyl imidazole and sulfonic acid groups were successfully introduced into the mesoporous acidic PILs.[43] To further determine the state of C, N and S elements, high-resolution XPS spectra were analyzed in detail. Fig. 1b showed two peaks at binding energies of 286.6 and 284.8 eV, corresponding to the valence states of C in the C–S and C–C bonds, respectively. This was characteristic of the sulfonic acid group on mesoporous acid-functionalized PILs. Fig. 1c showed that the peak positions of N 1s were 402 and 400.3 eV, which corresponded to the valence distribution of the N element in the N–C bond. This

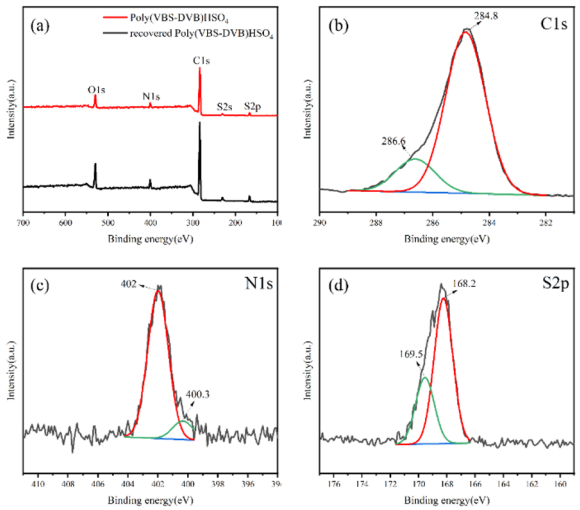

Fig. 1 XPS measurements of (a) wide-scan survey; (b) C 1s of Poly(VBS-DVB)HSO_4; (c) N 1s of Poly(VBS-DVB)HSO_4; (d) S 2p of Poly(VBS-DVB)HSO_4.

resulted from the quaternization of the imidazole ring and the 1,4-butane sulfonate lactone. As shown in Fig. 1d, S 2p had peaks at 169.5 and 168.2 eV, respectively, corresponding to the S in S–O. These XPS analyses further proved the successful synthesis of Poly(VBS-DVB)HSO_4.

Fig. 2a illustrated the FT-IR spectra of VBS, Poly(VBS-DVB), Poly(VBS-DVB)HSO_4 and recovered Poly(VBS-DVB)HSO_4. The peaks at 2925 cm^{-1} and 1459 cm^{-1} were assigned to the stretching vibration of C–H and imidazole ring C–N. The peaks at 1185 cm^{-1} and 1035 cm^{-1} were usually attributed to the asymmetric and symmetric stretching vibrations of sulfonic groups. The characteristic peak at 944 cm^{-1} was caused by the bending vibration of terminal group $=CH_2$ in the $HCR=CH_2$ structure. The disappearance of the characteristic peak of terminal group $HCR=CH_2$ proved the successful polymerization of PILs. In addition, the characteristic peak at 719 cm^{-1} was caused by the C–H out-of-plane bending vibration of the benzene ring, which proved the successful introduction of the cross-linker DVB in PILs.[44] And the peak at 1000 cm^{-1} assigned to the stretching vibration of the $-HSO_4$ group proved the success of anion exchange. It could be seen from the figure that the addition of H_2SO_4 might affect the absorption frequency of some functional groups. The peak values of the C–N bond (1449 cm^{-1}) of imidazole ring and the C–H bond (719 cm^{-1}) of benzene ring both decreased slightly. The $-HSO_4$ functional group (1000 cm^{-1}) of recovered Poly(VBS-DVB)HSO_4 showed signs of slight overlap with the characteristic peak of the sulfonic acid functional group. The recovered Poly(VBS-DVB)HSO_4 also had a slight effect on the absorption frequency of functional groups. However, the effect was weaker than Poly(VBS-DVB)HSO_4, which might be due to a small amount of sulfuric acid leaching. The FT-IR results showed that the sulfonic acid group and $-HSO_4$ group were well bound to Poly(VBS-DVB)HSO_4.

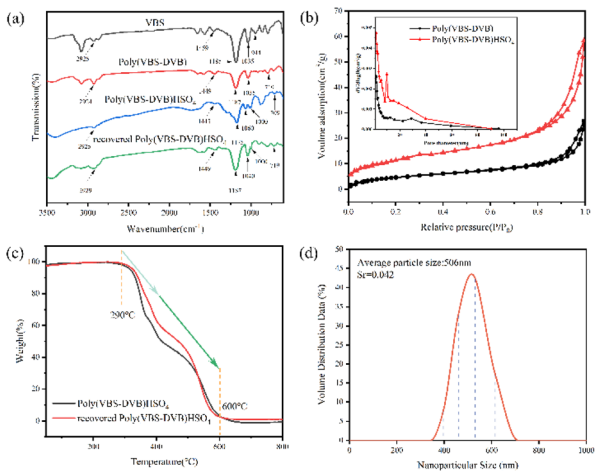

Fig. 2 (a) FT-IR spectra of VBS, Poly(VBS-DVB), Poly(VBS-DVB)HSO_4 and recovered Poly(VBS-DVB)HSO_4; (b) N_2 adsorption–desorption isotherms and pore size distribution curves of Poly(VMS-DVB) and Poly(VMS-DVB)HSO_4; (c) TG curves of Poly(VBS-DVB)HSO_4 and recovered Poly(VBS-DVB)HSO_4; (d) nanoparticle size distribution diagram of 506 nm.

The nitrogen adsorption and desorption isotherms of the samples were shown in Fig. 2b. It was obvious that both Poly(VMS-DVB) and Poly(VMS-DVB)HSO_4 showed type IV isotherms with a clear H1-type lag loop.[45] As could be seen from the figure, there was a clear capillary coalescence between p/p_0 = 0.8 and 1.0 with a sudden increase in adsorption and a hysteresis loop. The pore size distribution calculated by the Barrett–Joyner–Halenda (BJH) method showed that the pore channel distribution was mainly concentrated in the range of 2–40 nm, which was in the range of mesopore pore size. There were very few large pores. The specific surface areas of Poly(VBS-DVB) and Poly(VBS-DVB)HSO_4 were 17.9982 $m^2\ g^{-1}$ and 42.1907 $m^2\ g^{-1}$, and the pore volumes were 0.027 $cm^3\ g^{-1}$ and 0.065 $cm^3\ g^{-1}$, respectively. The specific data were shown in the Table S3.†

To investigate the thermal stability of the samples obtained, TG analysis was carried out as shown in Fig. 2c. The TGA curve dropped sharply from 290 °C to 600 °C with a weight loss of about 98%, which was due to the decomposition of the acidic functional groups and the polymer backbone.[45] Overall, Poly(VBS-DVB)HSO_4 have thermal stability at about 290 °C, and it is feasible to use them as catalysts.

Dynamic light scattering (DLS) is an important technical index to measure whether a substance belongs to nanomaterials or not.[46] The particle size of Poly(VBS-DVB)HSO_4 was characterized by Zetasizer Nano ZS90 (Fig. 2d). The average

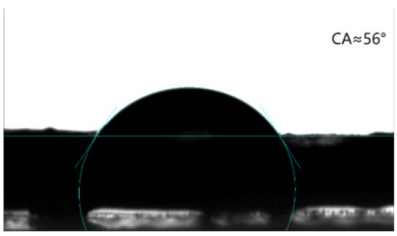

Fig. 3 The contact angle of water on the surface of Poly(VBS-DVB)HSO_4.

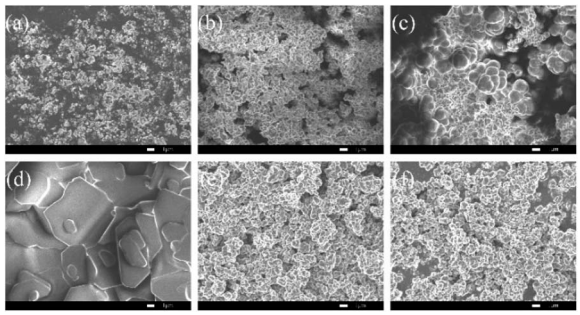

Fig. 4 Representative SEM images: Poly(VBS-DVB) was formed by different initiator dosage ((a) 1 wt%, (b) 3 wt%, (c) 10 wt%); (d) VBS; (e) Poly(VBS-DVB)HSO_4 (3 wt% initiator dosage); (f) recovered Poly(VBS-DVB)HSO_4 (3 wt% initiator dosage).

particle size of Poly(VBS-DVB)HSO_4 was 506 nm, and the relative standard deviation was Sr = 0.042. Fig. 3 showed the contact angle between Poly(VBS-DVB)HSO_4 and water, which was about 56°, with CA < 90° indicating that water wetted its solid surface more easily. The results indicated that in the hydrolysis reaction, the wettability of Poly(VBS-DVB)HSO_4 on the water was conducive to the better dispersion of the catalytic center.[44]

Fig. 4 was SEM images of representative samples. Fig. 4a–c were Poly(VBS-DVB) synthesized at the initiator dosage of 1 wt%, 3 wt% and 10 wt%, respectively. When the initiator dosage was too small, the pore distribution was uneven. While the initiator dosage was too large, the excessive polymerization occurred. Similar to the experimental results, when the initiator dosage was 3%, the pore size distribution was uniform, which was more conducive to the acid reaction. Fig. 4e and f were morphologically close to the images, indicating that Poly(VBS-DVB)HSO_4 inherited the morphology of Poly(VBS-DVB)HSO_4 precursor very well. The morphology of recovered Poly(VBS-DVB)HSO_4 did not change significantly, indicating that the structure of PILs was stable.

3.2. Experimental results and RSM analysis

3.2.1. RSM experiments and fitting the model. The experimental matrix was designed with Design-Expert 8.0 software, and 17 groups of parameter ratios were analyzed, which were composed of 12 factorial experiments and 5 central experimental. Table S4† showed the results of BBD. The predicted values for cyclohexanone oxime conversion were close to experimental ones in the acceptable variance range.

Analysis of variance (ANOVA) is an important step in response surface methodology to reveal the significance of each influence factor in the model fit, the reliability of the regression analysis and the accuracy of the regression equation, usually expressed in terms of *p*-value and *F*-value. Usually, the *p*-value of the model with cyclohexanone oxime conversion as the response target was <0.01, indicating that the relationship between the three influencing factors and the target value in the regression model was significant, and the model fit was high, with a certain degree of representativeness and high accuracy. From Table S5,† the *p*-value of Lack of Fit is >0.05, which indicated that the Lack of Fit is not significant. The test results were not greatly influenced by other factors, the test error was small, and the main influence point of the Lack of Fit was the number of central tests. In this experiment, five central tests were used to make the error randomly distributed in the test and improve the accuracy of a single test. The goodness of fit of the model can also be verified by multiple correlation coefficients. In this experiment, the multiple correlation coefficient $R^2 = 0.9817$, indicating that the influence of error was not obvious, and the regression equation was well fitted. The adjusted coefficient of determination adj$R^2 = 0.9582$, which meant that the model could explain 95.8% of the response value changes, and 4.2% of the total variation could not be explained by the model. The coefficient of variation of this model was CV = 4.13%, indicating good repeatability of the experiment. To sum up, the regression equation and the fitting model had high accuracy and authenticity and could be used as a reliable basis for subsequent analysis.

According to the *p*-values of the influence factors in Table S5,† the regression coefficients of catalyst amount and water consumption were less than 0.01, which meant that the influence is extremely significant, and the regression coefficient of reaction temperature was less than 0.05, which meant that the influence is significant. The *F*-values of the influencing factors (X_1, X_2, X_3) were 6.99, 126.2 and 38.92, respectively, indicating that the amount of catalyst had the greatest effect on the conversion of cyclohexanone oxime, followed by water consumption and reaction temperature. Among them, the partial regression coefficient of the interaction term X_2X_3 was very small, indicating that the interaction term of the interaction of the influencing factors catalyst dosage and water consumption had little effect on the conversion of cyclohexanone oxime. However, the significant coefficients of reaction temperature (X_{12}), catalyst amount (X_{22}) and water consumption (X_{32}) were less than 0.01, indicating that these three influencing factors had extremely significant effects on the conversion of cyclohexanone oxime. The quadratic response surface equation fitted by the Box–Behnken design method is:

$$Y = 73.66 + 2.34X_1 + 9.92X_2 + 5.51X_3 + 2.41X_1X_2 - 0.98X_1X_3 + 0.03X_2X_3 - 8.1X_1^2 - 11.51X_2^2 - 8.23X_3^2 \quad (5)$$

In the fitting formula (eqn (5)), Y is the conversion of cyclohexanone oxime, X_1 is the reaction temperature, X_2 is the amount of catalyst, and X_3 is the water consumption. From the formula, the first-order coefficients of reaction temperature, catalyst amount and water consumption were all positive, indicating that the positive increase of any two factors could make the target value increase positively.

3.2.2. Response surfaces. The 3D surface of the cyclohexanone oxime conversion model (eqn (5)) was plotted as a function of two process variables, while the last variable was kept at the zero level, which would facilitate understanding the interaction between the two experimental factors and identifying the optimal level from the plot. With the reaction time fixed at 1 h, the results of the effect of the three process variables on the reaction are shown in Fig. 5. The effect of the interaction

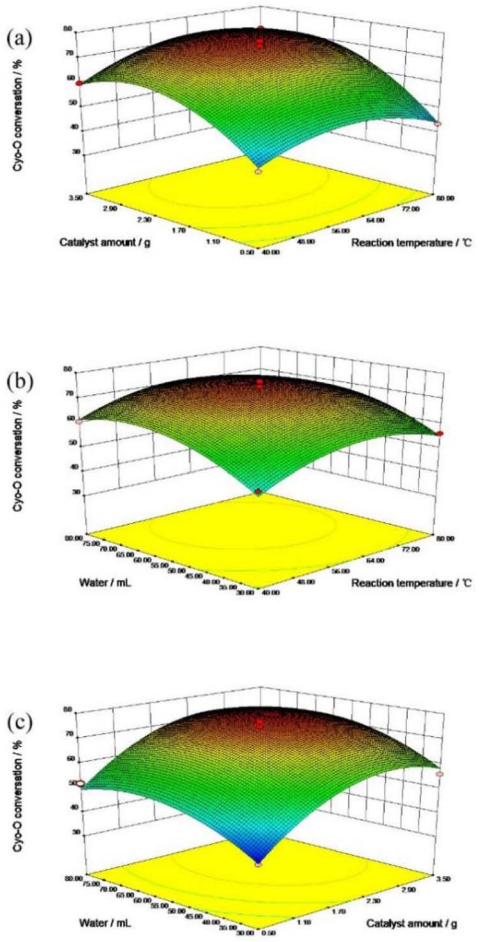

Fig. 5 Response surface diagram of cyclohexanone oxime conversion: (a) reaction temperature and catalyst amount, (b) reaction temperature and water consumption and (c) catalyst amount and water consumption.

between reaction temperature and catalyst amount was shown in Fig. 5a. With the rise of reaction temperature, the conversion of cyclohexanone oxime was increased first due to the increase in reaction temperature facilitating the positive hydrolysis reaction, passing through a maximum of nearly 68% at 60 °C, and then decreased again as a result of the reaction equilibrium constant K to shift in an exothermic direction.

As for the influence of catalyst amount, the cyclohexanone oxime conversion was increased gradually with the addition of catalyst amount. The more active centers the catalyst provided, the higher the reactants converted naturally. However, when the catalyst amount exceeded 2 g, the conversion of cyclohexanone oxime remained almost unchanged, indicating that the active center required for the reactants reached saturation.

Fig. 5b described the interaction between reaction temperature and water consumption. The conversion of cyclohexanone oxime elevated with the addition of reaction temperature and water consumption. An appropriate amount of water could accelerate the collision between the reactants and the catalyst molecules, thus promoting the reaction to proceed in the positive direction. However, excessive water would dilute the active center of the catalyst, thereby reducing the reaction conversion.

Fig. 5c demonstrated the interaction effect of catalyst dosage and water consumption. Within a certain range, increasing the amount of catalyst and water consumption promoted the reaction forward. Excessive water and catalyst were not conducive to the further conversion of cyclohexanone oxime.

To obtain the optimum conditions of cyclohexanone oxime conversion, the regression (eqn (5)) was solved. According to (eqn (5)), the optimal conditions were estimated as follows. When the reaction temperature was 65.38 °C, the amount of catalyst was 2.67 g, and the water consumption was 61.23 mL, the conversion of cyclohexanone oxime could reach 76.92%. To verify the validity of the model prediction, the experiment was carried out under the above conditions. The cyclohexanone oxime conversion was obtained at 77.23%. The experimental relative error was small, and the experimental value was not significantly different from the predicted value, indicating that the statistical model effectively predicted the conversion of cyclohexanone oxime.

3.3. Reusability of catalyst

As known to all, reusability is an important indicator of the catalyst's performance. It could be seen from Table S1† Poly(VBS-DVB)HSO_4 worked best was easy to recover, but its quality was slightly lost in the process of washing and transferring. To investigate the reusability of Poly(VBS-DVB)HSO_4, the reacted catalyst was separated by centrifugation after the first operation. The separated catalyst was washed repeatedly with ethanol and aqueous solution for more than three times to remove surface impurities. Next, the catalyst was filled into a column and rinsed with a certain concentration of H_2SO_4 solution (2.5 mol L^{-1}) for 5 min, and rinsed with CH_2Cl_2 to the pH value was about 7. The regenerated catalyst was vacuum dried at 80 °C for 6 h before the next turn, and Poly(VBS-DVB)HSO_4 remained well active after six cycles (Fig. 6). Elemental analysis found that the results of reactivated catalysts (C 31.55 wt%, H 4.89 wt%, N 1.26 wt%, S 10.03 wt%) and fresh catalysts were almost the same, which was consistent with the results of cyclic tests. It indicated that the acidic center on the surface of Poly(VBS-DVB)HSO_4 was relatively stable. The recovered Poly(VBS-DVB)HSO_4 was analyzed by FT-IR, XPS, and SEM, which was similar to that

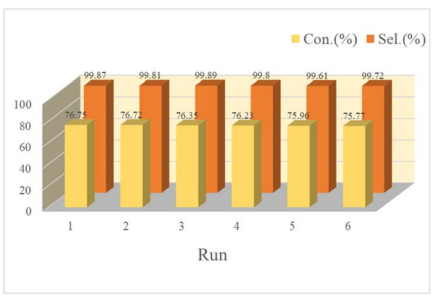

Fig. 6 Catalytic reusability of Poly(VBS-DVB)HSO_4 for hydrolysis of cyclohexanone oxime under optimal conditions.

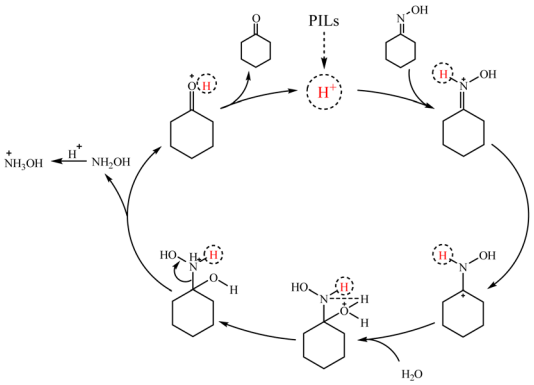

Scheme 2 Reduction of cyclohexanone oxime catalyzed by PILs.

of the fresh one. The FT-IR (Fig. 2a) and XPS (Fig. 1) of the recovered and fresh Poly(VBS-DVB)HSO_4 had no significant changes. For SEM results, both the recovered catalyst and the fresh catalyst (Fig. 4) maintained a spherical structure and no significant changes in the internal structure. It was demonstrated that Poly(VBS-DVB)HSO_4 was a catalyst with a stable structure and excellent catalytic performance.

Based on previous studies on the hydrolysis of oxime.[47,48] The possible mechanism of PILs catalyzed hydrolysis was also proposed as shown in Scheme 2. The reaction started with H^+ attacking the Brønsted acid site on the nitrogen atom of cyclohexanone oxime, followed by water attacking the α-carbon atom,[49] thus breaking the C=N bond. And then, hydrogen protons were transferred from water to nitrogen atoms.[50] In addition, the transition state further split into cyclohexanone(Fig. S1†),[51] H^+ and hydroxylamine[52] through C–N single bond breakage. The hydroxylamine was protonated to hydroxylamine salts (qualitative by potassium permanganate redox titration).

3.4. Catalytic activity of Poly(VBS-DVB)HSO_4 for the hydrolysis of different ketoximes

Based on the above results, a series of ketoximes were also examined including acetone oxime, butanone oxime, cyclopentanone oxime and acetophenone oxime. Table S6† gives the results. The experimental results revealed that Poly(VBS-DVB)HSO_4 exhibited excellent catalytic performance in all the hydrolysis reactions. The conversion of ketoxime was not less than 80.44%.

4. Conclusions

To sum up, in this paper, mesoporous acidic PILs were synthesized by free radical copolymerization of DVB and ILs. These materials were used as catalysts for hydrolysis of cyclohexanone oxime. The preparation conditions for the maximum conversion of cyclohexanone oxime were explored, and the maximum hydrolysis conversion was obtained by the Box–Behnken design. The optimized reaction conditions determined by RSM were catalyst amount 2.6 g, water consumption 61 mL, conducted at 65 °C for 1 h, at which the reaction conversion reached 77.23%. The Poly(VBS-DVB)HSO_4 catalyst exhibited excellent catalytic activity, good structural stability and easy recovery property. Additionally, a possible reaction pathway involving hydrogen protons was proposed for the present hydrolysis. Moreover, a series of ketoximes were also examined including acetone oxime, butanone oxime, cyclopentanone oxime and acetophenone oxime over Poly(VBS-DVB)HSO_4 catalyst. The results also showed excellent catalytic performance. And the conversion of ketoxime was not less than 80.44%. It provides a bright future for similar ketone oxime hydrolysis reactions.

Author contributions

Shanshan Zhao: methodology, formal analysis, data curation, writing – original draft, writing – review & editing. Zhengxiang Ma: formal analysis, methodology, supervision. Peng Cheng: formal analysis, supervision. Yanji Wang: resources, formal analysis. Xinqiang Zhao: resources, supervision. Qiusheng Yang: resources, supervision. Junqi Zhang: supervision. Dongsheng Zhang: conceptualization, validation, methodology, writing – review & editing, project administration, funding acquisition.

Conflicts of interest

There are no conflicts to declare.

Acknowledgements

This work is supported by the National Natural Science Foundation of China (21878069, 21646015, U20A20152) and the Natural Science Foundation of Hebei Province (B2016202335).

Notes and references

1 J. Zheng, Z. Li, D. Zhang, Q. Yang, X. Zhao, B. Zhang and Y. Wang, *J. Mol. Liq.*, 2022, **348**, 118407.
2 H. Ichihashi and H. Sato, *Appl. Catal., A*, 2001, **221**, 359–366.
3 D. Han, J. Wan, Y. Ma, Y. Wang, M. Huang, Y. Chen, D. Li, Z. Guan and Y. Li, *Chem. Eng. J.*, 2014, **256**, 316–323.
4 M. Takhi, C. Murugan, M. Munikumar, K. M. Bhaskarreddy, G. Singh, K. Sreenivas, M. Sitaramkumar, N. Selvakumar, J. Das, S. Trehan and J. Iqbal, *Bioorg. Med. Chem. Lett.*, 2006, **16**, 2391–2395.
5 F. Raschig, *US Pat.*, US1010177, 1911.
6 A. van Rooij, *Ambix*, 2007, **54**, 192–210.
7 J. Kurt and W. Karl, *US Pat.*, US27119778, 1955.
8 Y. Xu, Z. Li, L. Gao, D. Zhang, X. Zhao, S. Wang and Y. Wang, *Ind. Eng. Chem. Res.*, 2015, **54**, 1068–1073.
9 F. Zhao, K. You, C. Peng, S. Tan, R. Li, P. Liu, J. Wu and H. Luo, *Chem. Eng. J.*, 2015, **272**, 102–107.
10 C. Dong, K. Wang, J. Zhang and G. Luo, *Chem. Eng. Sci.*, 2015, **126**, 633–640.
11 L. David, R. Arturo and S. Aurora, *Ind. Eng. Chem. Res.*, 2016, **55**, 6586–6594.

12 C. Q. Chu, H. T. Zhao, Y. Y. Qi and F. Xin, *J. Mol. Model.*, 2013, **19**, 2217–2224.
13 M. Deetlefs, M. Fanselow and K. R. Seddon, *RSC Adv.*, 2016, **6**, 4280–4288.
14 P. N. Reddy, P. Padmaja, B. V Subba Reddy and G. Rambabu, *RSC Adv.*, 2015, **5**, 51035–51054.
15 K. Vijayakrishna, D. Mecerreyes, Y. Gnanou and D. Taton, *Macromolecules*, 2009, **42**, 5167–5174.
16 V. V Phatake, T. A. Gokhale and B. M. Bhanage, *J. Mol. Liq.*, 2021, **345**, 117008.
17 J. G. Huddleston, A. E. Visser, W. M. Reichert, H. D. Willauer, G. A. Broker and R. D. Rogers, *Green Chem.*, 2001, **3**, 156–164.
18 Q. Zhang, S. Zhang and Y. Deng, *Green Chem.*, 2011, **13**, 2619–2637.
19 N. A. Noorhisham, D. Amri, A. H. Mohamed, N. Yahaya, N. M. Ahmad, S. Mohamad, S. Kamaruzaman and H. Osman, *J. Mol. Liq.*, 2021, **326**, 115340.
20 G. Kaur, H. Kumar and M. Singla, *J. Mol. Liq.*, 2022, **351**, 118556.
21 H. Xu, J. Zhang, D. Zhang, Y. Guo and F. Wu, *Fuel*, 2021, **288**, 119655.
22 D. S. Karousos, O. C. Vangeli, C. P. Athanasekou, A. A. Sapalidis, E. P. Kouvelos, G. E. Romanos and N. K. Kanellopoulos, *Chem. Eng. J.*, 2016, **306**, 146–154.
23 J. Cheng, Y. Li, L. Hu, J. Liu, J. Zhou and K. Cen, *Fuel Process. Technol.*, 2018, **172**, 216–224.
24 L. Zhang, H. Yang and H. Zhang, *Microporous Mesoporous Mater.*, 2022, **342**, 112118.
25 K. Sun, Y. Shi, W. Xu, N. Potter, Z. Li and J. Zhu, *Chem. Eng. J.*, 2017, **313**, 336–344.
26 S. Wang, J. Liu, P. Cheng, Z. Li, D. Zhang, Q. Yang, X. Zhao and Y. Wang, *Z. Anorg. Allg. Chem.*, 2021, **647**, 742–750.
27 Q. Wang, M. Ge, X. Guo, Z. Li, A. Huang, F. Yang and R. Guo, *Appl. Catal., A*, 2021, **626**, 118350.
28 G. Durga, P. Kalra, V. K. Verma, K. Wangdi and A. Mishra, *J. Mol. Liq.*, 2021, **335**, 116540.
29 G. Wang, S. Zhuo, L. Wang, S. Fang and Y. Lin, *Sol. Energy*, 2012, **86**, 1546–1551.
30 B. Lin, L. Qiu, J. Lu and F. Yan, *Chem. Mater.*, 2010, **22**, 6718–6725.
31 M. Li, L. Wang, B. Yang, T. Du and Y. Zhang, *Electrochim. Acta*, 2014, **123**, 296–302.
32 A. Blasig, J. Tang, X. Hu, Y. Shen and M. Radosz, *Fluid Phase Equilib.*, 2007, **256**, 75–80.
33 P. G. Mineo, L. Livoti, M. Giannetto, A. Gulino, S. Lo Schiavo and P. Cardiano, *J. Mater. Chem.*, 2009, **19**, 8861–8870.
34 Y. Xiong, Y. Wang, H. Wang and R. Wang, *Polym. Chem.*, 2011, **2**, 2306–2315.
35 P. Zhao, Y. Leng and J. Wang, *Chem. Eng. J.*, 2012, **204**, 72–78.
36 E. H. Jeon, M. D. Nguyen, C. Il Chung, Y. J. Kim, H. S. Kim, M. Cheong and J. S. Lee, *Appl. Catal., A*, 2007, **332**, 65–69.
37 X. Lin, M. Li, Z. Chen, M. Li, Y. Huang and T. Qiu, *J. Cleaner Prod.*, 2021, **292**, 125967.
38 A. Gopakumar, L. Lombardo, Z. Fei, S. Shyshkanov, D. Vasilyev, A. Chidambaram, K. Stylianou, A. Züttel and P. J. Dyson, *J. CO_2 Util.*, 2020, **41**, 101240.
39 N. Sahiner, A. O. Yasar and N. Aktas, *Int. J. Hydrogen Energy*, 2016, **41**, 20562–20572.
40 J. Li, Y. Zhou, D. Mao, G. Chen, X. Wang, X. Yang, M. Wang, L. Peng and J. Wang, *Chem. Eng. J.*, 2014, **254**, 54–62.
41 S. M. Ghoreishian, K. Badii, M. Norouzi and K. Malek, *Appl. Surf. Sci.*, 2016, **365**, 252–262.
42 D. R. Pinheiro, R. de F. Neves and S. P. A. Paz, *Microporous Mesoporous Mater.*, 2021, **323**, 111250.
43 H. Gao, Y. Zhou, X. Sheng, S. Zhao, C. Zhang, J. Fang and B. Wang, *Appl. Catal., A*, 2018, **552**, 138–146.
44 F. Liu, L. Wang, Q. Sun, L. Zhu, X. Meng and F.-S. Xiao, *J. Am. Chem. Soc.*, 2012, **134**, 16948–16950.
45 Y. Feng, L. Li, X. Wang, J. Yang and T. Qiu, *Energy Convers. Manage.*, 2017, **153**, 649–658.
46 M. D. Green, D. Salas-de la Cruz, Y. Ye, J. M. Layman, Y. A. Elabd, K. I. Winey and T. E. Long, *Macromol. Chem. Phys.*, 2011, **212**, 2522–2528.
47 B. J. Gregory, R. B. Moodie and K. Kinetics, *J. Chem. Soc. B*, 1970, 1687–1692.
48 R. A. M. O'Ferrall, D. M. O'Brien and D. G. Murphy, *Can. J. Chem.*, 2000, **78**, 1594–1612.
49 F. Zhao, K. You, R. Li, S. Tan, P. Liu, J. Wu, Q. Ai and H. Luo, *Ind. Eng. Chem. Res.*, 2015, **54**, 819–823.
50 K. Hyodo, K. Togashi, N. Oishi, G. Hasegawa and K. Uchida, *Green Chem.*, 2016, **18**, 5788–5793.
51 H. Egberink and C. Van Heerden, *Anal. Chim. Acta*, 1980, **118**, 359–368.
52 M. F. Haley and K. Yates, *J. Org. Chem.*, 1987, **52**, 1817–1824.